Hindawi
Shock and Vibration
Volume 2017, Article ID 6851903, 14 pages
https://doi.org/10.1155/2017/6851903

Research Article

Investigation of Parametric Instability of the Planetary Gear under Speed Fluctuations

Xinghui Qiu,[1,2] Qinkai Han,[1] and Fulei Chu[1]

[1] *Department of Mechanical Engineering, Tsinghua University, Beijing 100084, China*
[2] *Beijing Institute of Space Launch Technology, Beijing 100076, China*

Correspondence should be addressed to Fulei Chu; chufl@mail.tsinghua.edu.cn

Received 11 February 2017; Accepted 15 June 2017; Published 21 August 2017

Academic Editor: Dumitru I. Caruntu

Planetary gear is widely used in engineering and usually has symmetrical structure. As the number of teeth in contact changes during rotation, the time-varying mesh stiffness parametrically excites the planetary gear and may cause severe vibrations and instabilities. Taking speed fluctuations into account, the time-varying mesh stiffness is frequency modulated, and therefore sideband instabilities may arise and original instabilities are significantly affected. Considering two different speed fluctuations, original and sideband instabilities are numerically and analytically investigated. A rotational lumped-parameter model of the planetary gear is developed, in which the time-varying mesh stiffness, input speed fluctuations, and damping are considered. Closed-form approximations of instability boundaries for primary and combination instabilities are obtained by perturbation analysis and verified by numerical analysis. The effects of speed fluctuations and damping on parametric instability are systematically examined. Because of the frequency modulation, whether a parametric instability occurs cannot be simply predicted by the planet meshing phase which is applicable to constant speed. Besides adjusting the planet meshing phase, speed fluctuation supplies a new thought to minimize certain instability by adjusting the amplitude or frequency of the speed fluctuation. Both original and sideband instabilities are shrunken by damping, and speed fluctuation further shrinks the original instability.

1. Introduction

Planetary gears are widely used in power transmission because of their compact design, high efficiency, and reduced noise. As the number of teeth in contact changes during rotation, gear mesh stiffness varies periodically with time. This parametric excitation is a primary source of vibration and noise, causing severe vibrations and instabilities under certain operating conditions [1]. When the parametric excitation interacts with clearance nonlinearity, complicated nonlinear behaviors such as jump phenomena and secondary resonances are observed in planetary gears [2, 3]. Moreover, when the planets are equally spaced or diametrically opposed, this structural symmetry will lead to structured vibration characteristics [4, 5], which has a great effect on the parametric instability of the planetary gear caused by time-varying gear mesh stiffness [6]. Therefore, it is of great significance to determine the operating conditions of parametric instability and identify parameters that minimize the occurrence.

Parametric instability in gear system with constant speed has been investigated extensively. Tordion and Gauvin [7] and Benton and Seireg [8] analyzed the instabilities of the same two-stage gear system but derived contradictory conclusions. Lin and Parker [9] clarified the conflict and derived simple design formulas to control particular instabilities. For planetary gears, the structural symmetry results in highly structured modal properties [4, 5]. Based on the unique properties and ignoring damping, Lin and Parker [6] obtained the expressions of instability boundaries with constant speed using the perturbation method. In practice, planet meshing phase rules are often applied to neutralize the resonant response where the mesh frequency is near a natural frequency [10–13]. Considering the elastic deformation of the ring gear, Parker and Wu [14] investigated the parametric instability with an elastic-discrete model.

The investigations mentioned above assume that the input rotating speed is constant. However, speed fluctuation is unavoidable in practice such as the engine output speed and

the wind speed and induces frequency modulation of the gear mesh stiffness in gear systems. Parametric instability of the single-mesh gear system under speed fluctuation has attracted more and more attention [15–17]. The instability boundaries are numerically and analytically determined, and different speed fluctuation types are considered. However, investigations on the parametric instability of planetary gears under speed fluctuations are relatively scarce. Ignoring damping, Qiu et al. [18] numerically calculated a primary instability of the planetary gear under engine speed fluctuation. Analytical expressions of parametric instabilities were not obtained, and the influence rules of fluctuation parameters on the instabilities were not derived.

The objective of this investigation is to systematically analyze the parametric instabilities induced by two different speed fluctuations and present a new way to control the parametric instability by adjusting speed fluctuation parameters. Perturbation analysis is conducted to determine operating conditions leading to instabilities and the results are verified by numerical integration. A pure rotational model of the planetary gear considering speed fluctuation and damping is introduced first. The parametric instabilities are then numerically and analytically investigated. Finally, the influences of various parameters on instabilities are investigated, such as the frequency and amplitude of speed fluctuations and system damping.

The main differences between this paper and [18] are the following: (1) two speed fluctuation types are considered, and their different influences on parametric instability are investigated; (2) damping is included in this paper, and the combined effect of damping and speed fluctuation is indicated; (3) besides numerical investigation, analytical expressions of primary and combination parametric instabilities are derived; (4) the influence rules of fluctuation amplitude and frequency on the instabilities are concluded, and a new way to adjust instability is presented.

2. System Model

The analysis deals with the parametric instability of the planetary gear subjected to input speed fluctuations. A rotational lumped-parameter model of the planetary gear is shown in Figure 1. All components are modeled as rigid bodies with moments of inertia I_c, I_r, I_s, and I_n ($n = 1, 2, \ldots, N, N$ is the number of planets). The subscripts c, r, s, and n denote the carrier, ring, sun, and the nth planet, respectively. The circumferential angle of the nth planet is represented by ψ_n. Only gear rotational displacements $u_h = r_h\varphi_h$ ($h = c, r, s, 1, \ldots, N$) are considered, where r_h is the base circle radius and φ_h are the rotations in radian. Sun-planet and ring-planet gear meshes are modeled as linear springs acting along the line of action and are denoted by $k_{sn}(t)$ and $k_{rn}(t)$, respectively.

For spur gears, gear mesh stiffness is usually approximated as rectangular wave and expressed in Fourier series as [6]

$$k_{sn}(t) = k_{sp} + 2k_{sv}\sum_{l=1}^{\infty}\left(a_{sn}^{(l)}\sin l\theta + b_{sn}^{(l)}\cos l\theta\right),$$
$$k_{rn}(t) = k_{rp} + 2k_{rv}\sum_{l=1}^{\infty}\left(a_{rn}^{(l)}\sin l\theta + b_{rn}^{(l)}\cos l\theta\right). \quad (1)$$

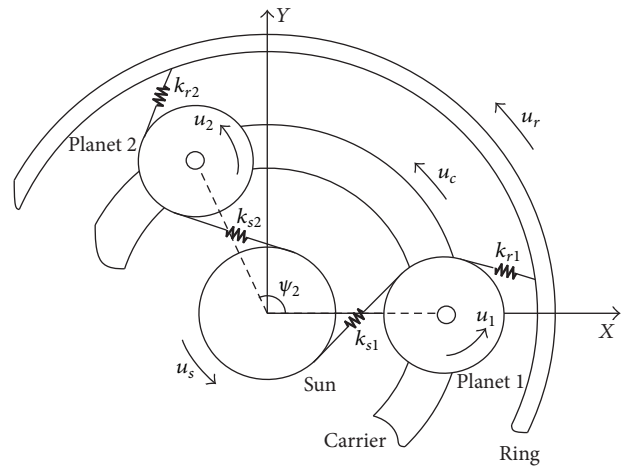

Figure 1: Rotational lumped-parameter model of the planetary gear.

The calculation of θ under input speed variation is stated in detail as follows. In general, the input speed for rigid body conditions can be introduced via the Fourier series as [18]

$$\Omega(t) = \Omega_0\left(1 + \alpha\cos\omega_a t\right), \quad (2)$$

where Ω_0 is the nominal input speed and a small parameter α is defined to indicate the amplitude of the speed fluctuation:

$$\theta = \int_0^t p\Omega(t)\,dt = \omega t + \beta\sin\left(\omega_a t\right). \quad (3)$$

In (3), $\omega = p\Omega_0$ is the nominal mesh frequency without considering the speed fluctuation, and $\beta = \alpha\omega/\omega_a$ depends on the amplitude of the speed fluctuation and the ratio between the nominal input speed and the fluctuation frequency. In planetary gear, p is determined by the configuration and the tooth number of the central gears. With a fixed ring, $p = Z_r$ when the carrier is the input element, and $p = Z_rZ_s/(Z_r+Z_s)$ when the sun is the input element. Substituting (3) into (1), sun-planet and ring-planet mesh stiffness can be rewritten as

$$k_{sn}(t) = k_{sp} + 2\varepsilon_1 k_{sp}\sum_{l=1}^{\infty}\left(a_{sn}^{(l)}\sin l\left(\omega t + \beta\sin\omega_a t\right) + b_{sn}^{(l)}\cos l\left(\omega t + \beta\sin\omega_a t\right)\right),$$
$$k_{rn}(t) = k_{rp} + 2\varepsilon_2 k_{rp}\sum_{l=1}^{\infty}\left(a_{rn}^{(l)}\sin l\left(\omega t + \beta\sin\omega_a t\right) + b_{rn}^{(l)}\cos l\left(\omega t + \beta\sin\omega_a t\right)\right), \quad (4)$$

where the two small parameters $\varepsilon_1 = k_{vs}/k_{sp}$ and $\varepsilon_2 = k_{vr}/k_{rp}$ are defined to indicate the amplitudes of the gear mesh stiffness variations. It can be clearly seen that the gear mesh stiffness is frequency modulated by the speed fluctuation. The time history and the spectrum of an example gear mesh stiffness under speed fluctuation are shown in Figure 2. Because of the frequency modulation induced by speed fluctuations, sideband frequencies are introduced and symmetrically distributed on both sides of the harmonics of the nominal

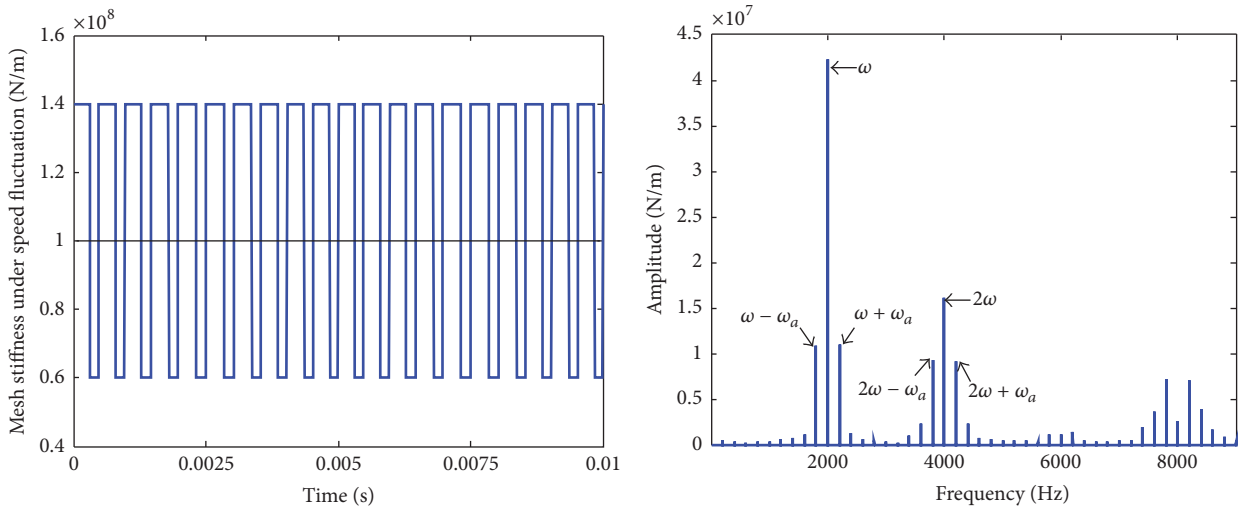

FIGURE 2: (a) Time history and (b) spectrum of an example sun-planet mesh stiffness under input speed fluctuation with $\omega = 2000$ Hz, $\omega_a = 200$ Hz, and $\beta = 0.5$.

gear mesh frequency ω, and the amplitude at nominal gear mesh frequency ω changes as well. In contrast to the single frequency excitation without considering speed fluctuations, more instability regions will arise due to sideband frequencies, and the original instability (which is similar to that of constant speed) will be affected.

Based on the relationship between the fluctuation frequency ω_a and the nominal gear mesh frequency ω, the input speed fluctuations can be classified into two categorizations: in the first type, the fluctuation frequency ω_a is constant; in the second type, fluctuation frequency ω_a is proportional to the nominal mesh frequency ω; that is, $\omega = P\omega_a$, such as the engine speed fluctuation [15, 16].

Through force analysis, the equations of motion of the planetary gear can be derived, and the system stability is governed by the free vibration equation [19]. The equation is applicable for general 2K-H planetary gear, and input and output component is not restricted:

$$\mathbf{M}\ddot{\mathbf{x}} + \mathbf{C}\dot{\mathbf{x}} + \mathbf{K}(t)\,\mathbf{x} = \mathbf{0}, \tag{5}$$

$$\mathbf{x} = \left[u_c, u_r, u_s, u_1, \ldots, u_N\right]^T, \tag{6}$$

$$\mathbf{M} = \operatorname{diag}\left[\frac{I_c}{r_c^2} + Nm_p, \frac{I_r}{r_r^2}, \frac{I_s}{r_s^2}, \frac{I_1}{r_1^2}, \ldots, \frac{I_N}{r_N^2}\right], \tag{7}$$

$$\mathbf{K}(t) = \begin{bmatrix} \sum_{n=1}^{N}\left(\widetilde{k}_{sn}\cos\alpha_s + \widetilde{k}_{rn}\cos\alpha_r\right) & -\sum_{n=1}^{N}\widetilde{k}_{rn} & -\sum_{n=1}^{N}\widetilde{k}_{sn} & \widetilde{k}_{r1} - \widetilde{k}_{s1} & \widetilde{k}_{r2} - \widetilde{k}_{s2} & \cdots & \widetilde{k}_{rN} - \widetilde{k}_{sN} \\ & \sum_{n=1}^{N}k_{rn} & 0 & -k_{r1} & -k_{r2} & \cdots & -k_{rN} \\ & & \sum_{n=1}^{N}k_{sn} & k_{s1} & k_{s2} & \cdots & k_{sN} \\ & & & k_{r1} + k_{s1} & 0 & \cdots & 0 \\ & \text{symmetric} & & & k_{r2} + k_{s2} & \cdots & 0 \\ & & & & & \ddots & \vdots \\ & & & & & & k_{rN} + k_{sN} \end{bmatrix}, \tag{8}$$

$$\begin{aligned} \widetilde{k}_{sn} &= k_{sn}(t)\cos\alpha_s, \\ \widetilde{k}_{rn} &= k_{rn}(t)\cos\alpha_r. \end{aligned} \tag{9}$$

Table 1: Simulation parameters of an example planetary gear with three equally spaced and in-phase planets.

Number of planets	$N = 3$
Inertia (kg)	$\frac{I_s}{r_s^2} = 2.5, \frac{I_s}{r_s^2} = 2.5, \frac{I_p}{r_p^2} = 2$
Mesh stiffness (N/m)	$k_{sp} = k_{rp} = 10^8$
Pressure angle (degree)	$\alpha_s = 24.6, \alpha_r = 20.19$
Contact ratio	$c_s = 1.4, c_r = 1.6$
Circumferential angle	$\psi_n = \frac{2\pi(n-1)}{N}, \ n = 1, 2, \ldots, N$
Sun-planet meshing phase	$\gamma_{sn} = [0, 0, 0]$
Ring-planet meshing phase	$\gamma_{rn} = [0, 0, 0]$
Natural frequencies (Hz)	$\omega_1 = 0, \omega_2 = 1177.7, \omega_3 = \omega_4 = 1591.5, \omega_5 = 2215.1$
Mesh stiffness variation	$\varepsilon = \varepsilon_1 = 0, 0.05, 0.1, 0.15, 0.2, 0.25$

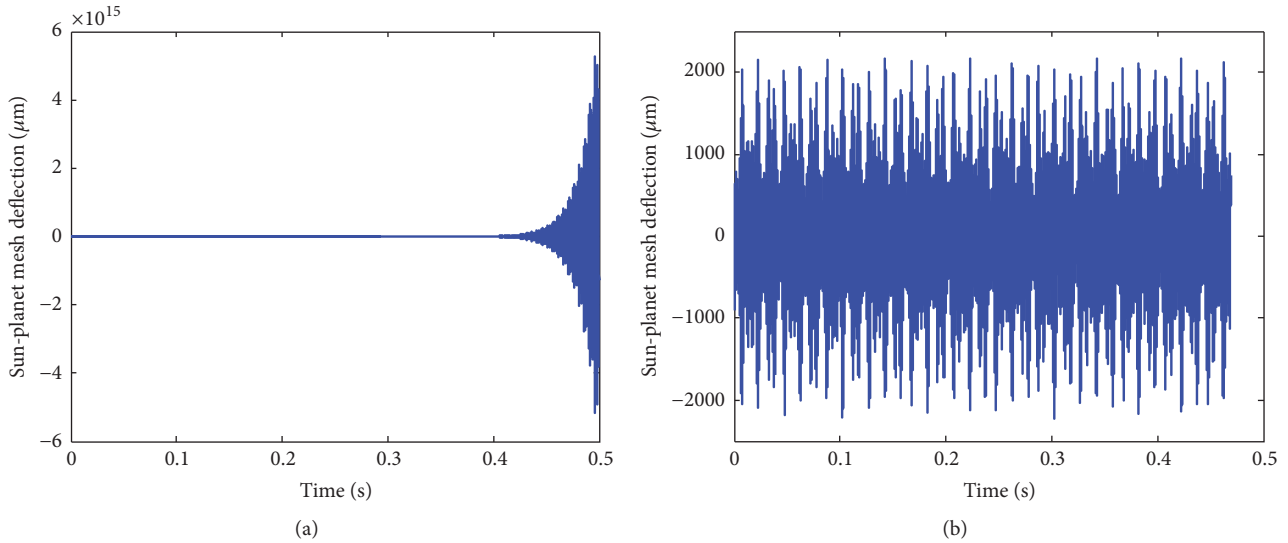

Figure 3: Sun-planet mesh deflections for $\alpha = 0.05$, $\varepsilon = 0.15$, and $\omega_a = 200$ Hz at nominal mesh frequencies of (a) 4000 Hz and (b) 4265 Hz.

Substituting (4) into (9) and letting $\varepsilon = \varepsilon_1 = \varepsilon_2 c_r / c_s$ (c_r and c_s are contact ratios), the time-varying stiffness matrix can be rewritten as

$$\mathbf{K}(t) = \mathbf{K}_0 + 2\varepsilon \sum_{l=1}^{\infty} \left(\mathbf{K}_{v1}^{(l)} \sin l\theta + \mathbf{K}_{v2}^{(l)} \cos l\theta \right), \tag{10}$$

where $\mathbf{K}_0$ is the time-invariant stiffness matrix with the inclusion of the average gear mesh stiffness and $\mathbf{K}_{v1}^{(l)}$ and $\mathbf{K}_{v2}^{(l)}$ are the Fourier coefficient matrices. Damping is introduced via the modal damping ratio and expressed as

$$\mathbf{C} = \left(\mathbf{V}^{-1} \right)^T \operatorname{diag}\left(2\xi_j \omega_j \right) \mathbf{V}^{-1}, \tag{11}$$

where ξ_j ($j = 1, 2, \ldots, N + 3$) are the modal damping ratios. The modal matrix $\mathbf{V}$ and the natural frequencies ω_j are calculated by solving the eigenvalue problem $\mathbf{K}_0 \mathbf{v}_j = {\omega_j}^2 \mathbf{M} \mathbf{v}_j$. The vibration matrix $\mathbf{V}$ is normalized as $\mathbf{V}^T \mathbf{M} \mathbf{V} = \mathbf{I}$ [19].

3. Numerical Analysis

In the case of steady speed, parametric instability occurs in the vicinity of the critical frequencies defined as $\omega/(\omega_m + \omega_d) = 2/q$ ($q = 1, 2, 3, \ldots$), where ω_m and ω_d are the natural frequencies of the planetary gear [6]. If $m = d$, the situation is defined as primary instability. If $m \neq d$, the situation is defined as combination instability. As high-order instabilities have much smaller instability regions and are unlikely to occur in practice [6], the following analysis focuses on $q = 1$.

An example planetary gear with equally spaced and in-phase planets is used for numerical simulation. The ring is fixed to the gearbox housing, and its vibration is constrained to be zero. Damping is ignored for the example numerical analysis. Simulation parameters are listed in Table 1. The operating conditions leading to parametric instabilities can be derived by calculating the free vibrations under nontrivial initial conditions using numerical integration. As shown in Figure 3, if the amplitude of the response diverges, the response is unstable. Otherwise, the response is stable. Based

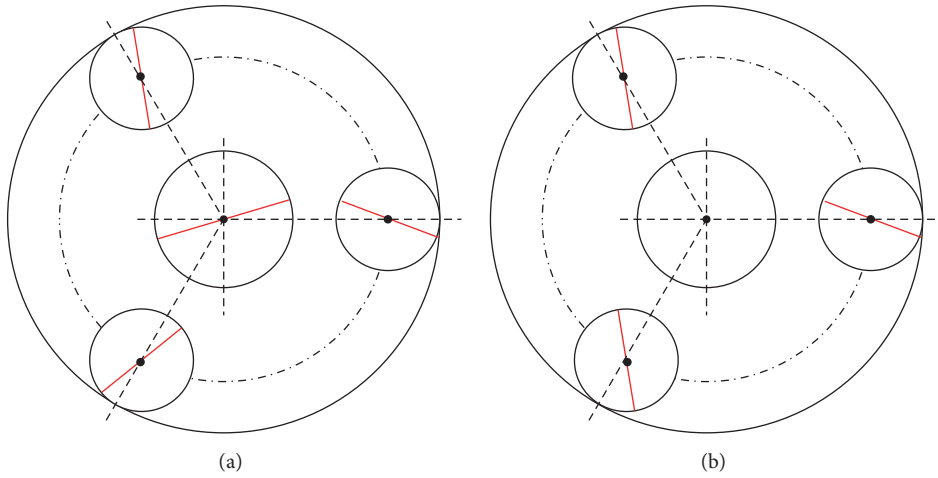

Figure 4: Modal properties of the planetary gear with three equally spaced planets: (a) distinct mode; (b) degenerate mode. Dashed lines are the equilibrium positions and solid lines are the deflected positions.

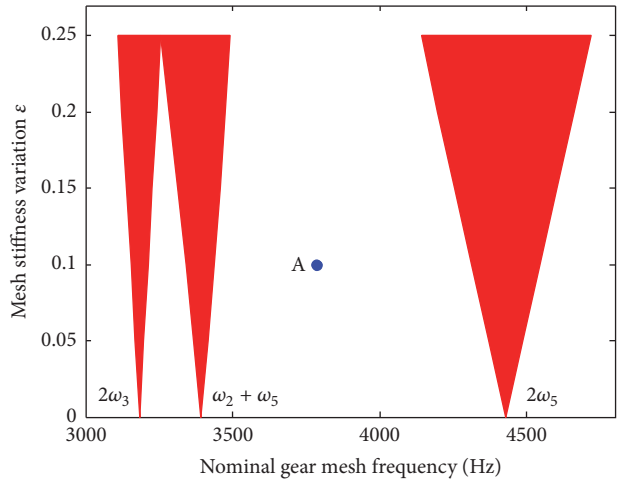

Figure 5: Stability diagram of the example planetary gear for constant input speed.

on this, the instability regions of the planetary gear under two different speed fluctuations can be numerically obtained.

Because of the unique cyclic symmetry, the vibration modes of the planetary gear with three equally spaced planets can be classified into 1 rigid body mode (ω_1), 2 distinct modes (ω_2, ω_5), and 2 degenerate modes ($\omega_3 = \omega_4$). As shown in Figure 4, the planets have identical motions in the distinct modes, and the central components have no motions and the motions of the planets differ in the degenerate modes.

Because of this unique modal property, whether certain instability occurs under constant speed can be directly estimated by planet meshing phase [6]: when the planet meshes are sequentially phased, primary instability and combination instability of the distinct modes are suppressed; when the planet meshes are in-phase, combination instability of distinct and degenerate mode is suppressed. Therefore, for the example planetary gear with in-phase planets, parametric instability does not occur in the vicinity of $\omega_2 + \omega_3$ and $\omega_3 + \omega_5$ without considering speed fluctuation, as shown in Figure 5.

Responses of the planetary gear at point A (ω = 3787 Hz which is in the vicinity of $\omega_3 + \omega_5$) in the presence of speed fluctuation are compared with those for constant speed. For constant speed, the vibration displacement and spectral amplitudes converge, as shown in Figure 6. That is, parametric instability does not occur at point A for constant speed. Because of the influence of the frequency modulation induced by speed fluctuations, instability may occur in the frequency range where no instability occurs under constant speed. As shown in Figure 7, parametric instability occurs at point A with the inclusion of speed fluctuation. Compared with the constant speed case shown in Figure 6(b), more frequency components occur in the power spectrum, and the spectral amplitude increases with time. Therefore, whether instability occurs at certain nominal gear mesh frequency cannot be simply predicted by the planet meshing phase.

The stability diagrams in the vicinity of $2\omega_5$ for two different speed fluctuations are shown in Figure 8. The width of original instability which is similar to that of the constant

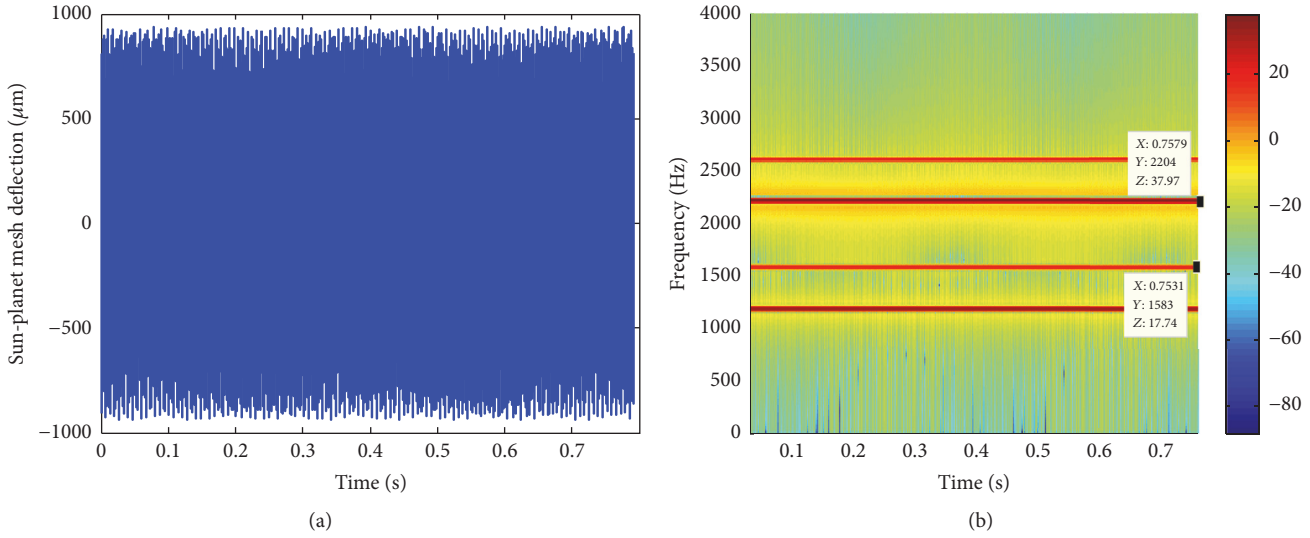

Figure 6: Dynamic response of the planetary gear at point A: (a) time history; (b) power spectrum.

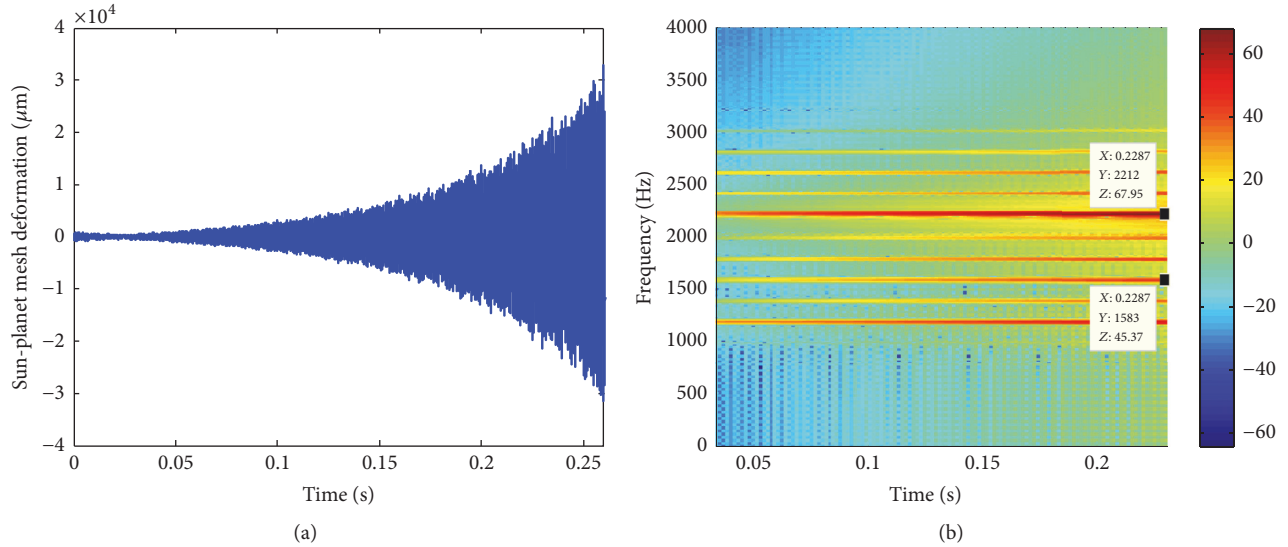

Figure 7: Dynamic response of the planetary gear at point A for $\alpha = 0.05$ and $\omega_a = 200$ Hz: (a) time history; (b) power spectrum.

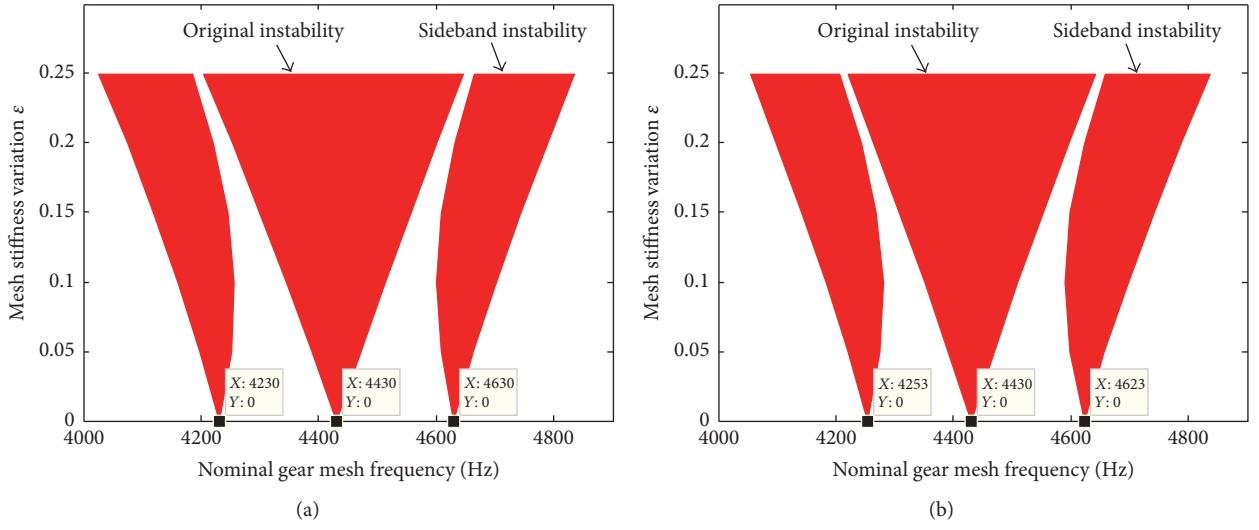

Figure 8: Stability diagrams of the example planetary gear in the vicinity of $2\omega_5$ for $\alpha = 0.05$: (a) $\omega_a = 200$ Hz; (b) $P = 24$.

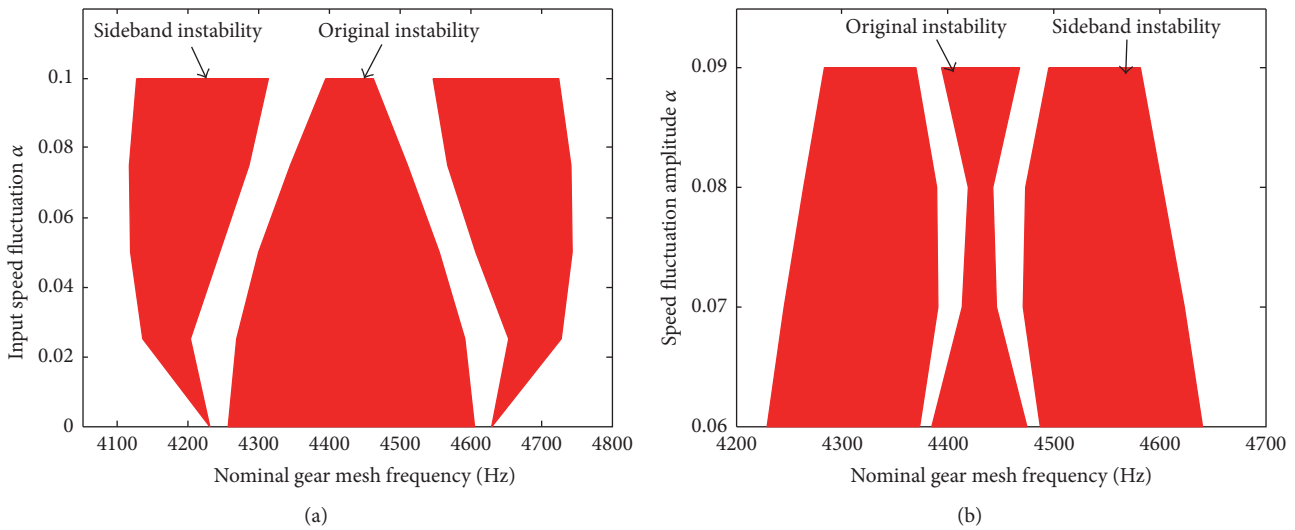

FIGURE 9: Variations of the instabilities in the vicinity of $2\omega_5$ with the speed fluctuation amplitude α for $\varepsilon = 0.15$: (a) $\omega_a = 200$ Hz; (b) $P = 40$.

speed case is changed, and sideband instabilities arise as well. These changes are closely related to the frequency modulation of the gear mesh stiffness [17]: (1) the amplitude at nominal mesh frequency changes; (2) sideband frequencies have influence on original instability and may be in the frequency range of parametric resonance, generating sideband instabilities. Comparing Figure 8(a) with Figure 8(b), it can be clearly seen that the original instability is approximately symmetrical, while the sideband instability at higher frequencies leans to high frequency direction and that at lower frequencies leans to low frequency direction. Moreover, the distributions of instabilities for the two fluctuations are different. For constant speed fluctuation frequency ω_a, the sideband instabilities are equally spaced around the original instabilities and the interval is ω_a, while for $\omega = P\omega_a$, sideband instabilities distribute more densely in the low frequency region.

The characteristics of the speed fluctuation have a great effect on the widths of the instability regions when planet meshing phases are determined, and the influence rule is closely related to the amplitude and frequency of the speed fluctuation. As shown in Figure 9(a), the sideband instabilities increase with the speed fluctuation amplitude α, while the original instability decreases with the speed fluctuation amplitude α. As shown in Figure 9(b), the original instability is relatively small and first decreases and then increases with the speed fluctuation amplitude α. The phenomena shown in Figure 9 inspire a new thought to decrease the instabilities of the planetary gear with the inclusion of the speed fluctuation. In order to systematically investigate the parametric instability of the planetary gear under speed fluctuation and present a new way to control instabilities, analytical investigation is conducted using the method of multiple scales (MMS).

4. Perturbation Analysis

Substituting the modal transformation $\mathbf{x} = \mathbf{V}\mathbf{z}$ into (5), the free vibrations of the planetary gear with a fixed ring are transformed into modal response and are expressed as

$$\ddot{z}_i + \varepsilon\lambda_i\dot{z}_i + \omega_i^2 z_i + 2\varepsilon\sum_{w=2}^{N+2}\sum_{l=1}^{\infty}\left(D_{iw}^{(l)}\sin l\theta + E_{iw}^{(l)}\cos l\theta\right)z_w = 0, \quad i = 2,\ldots,N+2, \tag{12}$$

where the matrices $\mathbf{D}^{(l)} = \mathbf{V}^T\mathbf{K}_{v1}^{(l)}\mathbf{V}$ and $\mathbf{E}^{(l)} = \mathbf{V}^T\mathbf{K}_{v2}^{(l)}\mathbf{V}$ and $\varepsilon\lambda_i = 2\xi_i\omega_i$. Because $i = 1$ responds to the rigid body mode which does not affect the parametric instability of the planetary gear, it is not considered in the following analysis. Using the method of multiple scales, the solutions of (12) can be expressed as [19, 20]

$$z_i = z_{i0}(t_0, t_1, \ldots) + \varepsilon z_{i1}(t_0, t_1, \ldots) + \cdots, \quad i = 2,\ldots,N+2, \tag{13}$$

where $t_0 = t$ and $t_1 = \varepsilon t$. Substituting (13) into (12) and making the coefficients of the same power in ε of both sides equal yield

$$D_0^2 z_{i0} + \omega_i^2 z_{i0} = 0, \tag{14}$$

$$D_0^2 z_{i1} + \omega_i^2 z_{i1} = -2D_0D_1z_{i0} - \lambda_i D_0 z_{i0} - 2\sum_{w=2}^{N+2}\sum_{l=1}^{\infty}\left(D_{iw}^{(l)}\sin l\theta + E_{iw}^{(l)}\cos l\theta\right)z_{w0}. \tag{15}$$

The general solutions of (14) are

$$z_{i0} = A_i(t_1)\, e^{j\omega_i t} + \text{c.c.} \quad i = 2, \ldots, N+2, \tag{16}$$

where c.c. represents the complex conjugate of the preceding terms. Because of speed fluctuations, $\sin(\theta)$ and $\cos(\theta)$ are no longer the standard Fourier series. With the aid of the Bessel function of the first kind [21], they can be expanded in generalized Fourier series as

$$\begin{aligned}\sin\theta &= J_0(\beta)\sin\omega t + \sum_{m=1}^{\infty} J_{2m}(\beta)\left[\sin(\omega + 2m\omega_a)t\right.\\ &\left. + \sin(\omega - 2m\omega_a)t\right] + \sum_{m=0}^{\infty} J_{2m+1}(\beta)\\ &\cdot\left[\sin(\omega + (2m+1)\omega_a)t\right.\\ &\left. - \sin(\omega - (2m+1)\omega_a)t\right],\end{aligned} \tag{17}$$

$$\begin{aligned}\cos\theta &= J_0(\beta)\cos\omega t + \sum_{m=1}^{\infty} J_{2m}(\beta)\left[\cos(\omega + 2m\omega_a)t\right.\\ &\left. + \cos(\omega - 2m\omega_a)t\right] + \sum_{m=0}^{\infty} J_{2m+1}(\beta)\\ &\cdot\left[\cos(\omega + (2m+1)\omega_a)t\right.\\ &\left. - \cos(\omega - (2m+1)\omega_a)t\right].\end{aligned} \tag{18}$$

Substitution of (16) and (18) into (15) yields

$$\begin{aligned}D_0^2 z_{i1} + \omega_i^2 z_{i1} &= -2j\omega_i e^{j\omega_i t} D_1 A_i - \lambda_i j\omega_i e^{j\omega_i t} A_i\\ &- \sum_{w=2}^{N+2}\sum_{l=1}^{\infty} A_w J_0(\beta)\left[\left(E_{iw}^{(l)} - jD_{iw}^{(l)}\right)e^{j(\omega_w + l\omega)t}\right.\\ &\left. + \left(E_{iw}^{(l)} + jD_{iw}^{(l)}\right)e^{j(\omega_w - l\omega)t}\right] - \sum_{w=2}^{N+2}\sum_{l=1}^{\infty}\sum_{m=1}^{\infty} J_m(\beta)\\ &\cdot A_w\left[\left(E_{iw}^{(l)} - jD_{iw}^{(l)}\right)e^{j(\omega_w + l(\omega + m\omega_a))t} + \left(E_{iw}^{(l)} + jD_{iw}^{(l)}\right)\right.\\ &\left.\cdot e^{j(\omega_w - l(\omega + m\omega_a))t}\right] - \sum_{w=2}^{N+2}\sum_{l=1}^{\infty}\sum_{m=1}^{\infty} J_m(\beta)\\ &\cdot A_w\left[\left(E_{iw}^{(l)} - jD_{iw}^{(l)}\right)e^{j(\omega_w + l(\omega - m\omega_a))t}\right.\\ &\left. + \left(E_{iw}^{(l)} + jD_{iw}^{(l)}\right)e^{j(\omega_w - l(\omega - m\omega_a))t}\right] + \text{c.c.}\end{aligned} \tag{19}$$

In the following perturbation analysis, primary instabilities of distinct modes, primary instabilities of degenerate modes, and combination instabilities of distinct modes are considered. Other instabilities can be obtained following the similar procedure listed below.

(1) Primary Instability of Distinct Modes. Let $l\omega + n\omega_a = 2\omega_p + \varepsilon\sigma$ $(n = 0, \pm1, \pm2, \ldots)$, where ω_p is distinct and σ is the detuning parameter to be determined. Elimination of secular terms in (19) requires

$$\begin{aligned}&2j\omega_p D_1 A_p + \lambda_p j\omega_p A_p\\ &\quad + J_n(\beta)\,\overline{A}_p\left(E_{pp}^{(l)} - jD_{pp}^{(l)}\right)e^{j\sigma t_1} = 0.\end{aligned} \tag{20}$$

Substitution of $A_p(t_1) = (1/2)a(t_1)e^{j\beta(t_1)} + \text{c.c.}$ into (20) yields

$$\begin{aligned}&\omega_p D_1 a + \frac{1}{2}a\omega_p\lambda_p - \frac{1}{2}aJ_n(\beta)\left(D_{pp}^{(l)}\cos\gamma - E_{pp}^{(l)}\sin\gamma\right)\\ &\quad = 0,\\ &\omega_p D_1\gamma - \omega_p\sigma + J_n(\beta)\left(E_{pp}^{(l)}\cos\gamma + D_{pp}^{(l)}\sin\gamma\right) = 0,\end{aligned} \tag{21}$$

where $\gamma = \sigma t_1 - \beta$. To obtain the steady-state motion, let $D_1 a = D_1\gamma = 0$, and then σ can be determined:

$$\sigma = \pm\frac{\sqrt{J_n^2(\beta)\left(\left(E_{pp}^{(l)}\right)^2 + \left(D_{pp}^{(l)}\right)^2\right) - \lambda_p^2\omega_p^2}}{\omega_p}. \tag{22}$$

If the speed fluctuation frequency ω_a is proportional to the nominal gear mesh frequency ω, $\beta = \alpha P$ does not change with ω, and thus the instability boundaries can be easily expressed as

$$\begin{aligned}&\omega\\ &= \frac{\left(2\omega_p \pm \left(\sqrt{\varepsilon^2 J_0^2(\alpha P)\left(\left(E_{pp}^{(l)}\right)^2 + \left(D_{pp}^{(l)}\right)^2\right) - 4\xi_p^2\omega_p^4}\right)/\omega_p\right)}{(l + n/P)}.\end{aligned} \tag{23}$$

If ω_a is constant, $\beta = \alpha\omega/\omega_a$ varies with ω, and the instability boundaries can be obtained by solving the following equation:

$$\begin{aligned}&l\omega + n\omega_a\\ &= 2\omega_p \pm \frac{\sqrt{\varepsilon^2 J_n^2(\beta)\left(\left(E_{pp}^{(l)}\right)^2 + \left(D_{pp}^{(l)}\right)^2\right) - 4\xi_p^2\omega_p^4}}{\omega_p}.\end{aligned} \tag{24}$$

The case $n = 0$ corresponds to the original instability, and the cases $n \neq 0$ correspond to sideband instabilities. From (23) and (24), it can be seen that the intersections of instability boundaries and the abscissa axis are $2\omega_0/(1 + n/P)$ and $2\omega_0 - n\omega_a$, respectively, which explains the different distributions of instabilities for the two fluctuation types. Moreover, with the increase of ω_a, the interval of original and sideband instability becomes larger. With the increase of P, the original and sideband instability region becomes more intense.

Once the detuning parameter σ is determined, the calculations of the instability boundaries are similar for all instabilities. Therefore, only the calculation of σ is emphasized in the following analysis.

(2) Combination Instability of Distinct Modes. Let $l\omega + n\omega_a = \omega_p + \omega_q + \varepsilon\sigma$ $(n = 0, \pm1, \pm2, \ldots)$, where ω_p and ω_q are both distinct. Elimination of secular terms in (19) requires

$$\begin{aligned}&2j\omega_p D_1 A_p + \lambda_p j\omega_p A_p\\ &\quad + J_n(\beta)\,\overline{A}_q\left(E_{pq}^{(l)} - jD_{pq}^{(l)}\right)e^{j\sigma t_1} = 0,\end{aligned}$$

$$2j\omega_q D_1 A_q + \lambda_q j\omega_q A_q + J_n(\beta)\overline{A}_p\left(E_{qp}^{(l)} - jD_{qp}^{(l)}\right)e^{j\sigma t_1} = 0. \tag{25}$$

Substituting $A_p(t_1) = (1/2)a_p(t_1)e^{j\beta_p(t_1)}$ + c.c. and $A_q(t_1) = (1/2)a_q(t_1)e^{j\beta_q(t_1)}$ + c.c. into (25), the detuning parameter σ is derived as

$$\sigma = \pm\sqrt{\frac{(1/4)J_0^2(\beta)\left(\left(E_{pq}^{(l)}\right)^2 + \left(D_{pq}^{(l)}\right)^2\right)\left(\sqrt{\lambda_p/\lambda_q} + \sqrt{\lambda_q/\lambda_p}\right)^2 - (1/4)\left(\lambda_p + \lambda_q\right)^2\omega_p\omega_q}{\omega_p\omega_q}}. \tag{26}$$

(3) Primary Instability of Degenerate Modes. Let $l\omega + n\omega_a = \omega_p + \omega_q + \varepsilon\sigma$ ($n = 0, \pm1, \pm2, \ldots$), where $\omega_p = \omega_q$ are degenerate. Elimination of secular terms in (19) requires

$$\begin{aligned} &2j\omega_p D_1 A_p + \lambda_p j\omega_p A_p + J_n(\beta) \\ &\quad\cdot\left[\overline{A}_p\left(E_{pp}^{(l)} - jD_{pp}^{(l)}\right) + \overline{A}_q\left(E_{pq}^{(l)} - jD_{pq}^{(l)}\right)\right]e^{j\sigma t_1} = 0, \\ &2j\omega_q D_1 A_q + \lambda_q j\omega_q A_q + J_n(\beta) \\ &\quad\cdot\left[\overline{A}_p\left(E_{qp}^{(l)} - jD_{qp}^{(l)}\right) + \overline{A}_q\left(E_{qq}^{(l)} - jD_{qq}^{(l)}\right)\right]e^{j\sigma t_1} = 0. \end{aligned} \tag{27}$$

Because modal coupling between the degenerate modes is stronger than that between distinct modes, the determination of the instability boundaries is more complex, as shown in (27). Following the standard procedure, the detuning parameter is expressed as

$$\sigma = \pm\frac{\sqrt{J_n^2(\beta)\Gamma^{(l)} - \lambda_p^2\omega_p^2}}{\omega_p}, \tag{28}$$

$$\Gamma^{(l)} = D_{pq}^{(l)}D_{qp}^{(l)} + E_{pq}^{(l)}E_{qp}^{(l)} + \frac{1}{2}\left(\left(D_{pp}^{(l)}\right)^2 + \left(D_{qq}^{(l)}\right)^2 + \left(E_{pp}^{(l)}\right)^2 + \left(E_{qq}^{(l)}\right)^2\right). \tag{29}$$

To validate the analytical results, comparisons of the numerical and analytical results using the same parameters are shown in Figure 10. It can be clearly seen that the perturbation solution for the original instabilities matches well with the numerical results for the two speed fluctuation types.

5. Discussions

5.1. Influence of Speed Fluctuations. As shown in (22), (26), and (29), planet meshing phase changes the instability regions by influencing the elements of matrices **D** and **E**. Besides planet meshing phase, it can be clearly seen that speed fluctuations have a significant influence on the width of instability region by changing the value of $J_n(\beta)$. That is, speed fluctuation amplitude α and frequency ω_a have a combined effect on the parametric instability width, and the influence rule is closely related to the properties of the Bessel function of the first kind.

As shown in Figure 11, $J_0(\beta)$ shows cosine oscillation attenuation, while the rest shows sine oscillation attenuation. This property explains the variation tendency of the original and sideband instabilities in the numerical analysis. For the first speed fluctuation type, where the speed fluctuation frequency ω_a is constant, the influences of α and ω_a on original instabilities in the vicinity of $2\omega_3$, $\omega_3 + \omega_5$, and $2\omega_5$ are shown in Figure 12. All original instabilities decrease with the increase of α and increase with the increase of ω_a under the simulation conditions. Because ω_a is constant, the ratio of the nominal mesh frequency ω and ω_a varies with ω. The change of instability width differs in different frequency range. With the definition of instability ratio ir = width ($\alpha \neq 0$)/width ($\alpha = 0$), the instability ratios of $2\omega_3$, $\omega_3 + \omega_5$, and $2\omega_5$ for $\omega_a = 200$ Hz and $\alpha = 0.05$ are 0.852, 0.826, and 0.715, respectively.

For the second speed fluctuation type, where $\omega = P\omega_a$, the influences of fluctuation amplitude α and frequency ratio P on original instabilities of $2\omega_3$, $\omega_3 + \omega_5$, and $2\omega_5$ are shown in Figure 13. Similarly, all original instabilities decrease with the increase of α and P under the simulation conditions. Because the frequency ratio P does not change with the nominal gear mesh frequency, instability ratios of $2\omega_3$, $\omega_3 + \omega_5$, and $2\omega_5$ are identical once the fluctuation amplitude is determined, which is different from the first fluctuation type.

Through the above parameter analysis, it can be found that the properties of the Bessel function of the first kind with different order supply a new possibility to minimize certain parametric instability by adjusting the parameters of the speed fluctuation. The adjusting rule is to minimize the value of $J_n(\beta)$: $n = 0$ corresponds to the original instability, and $n = \pm1, \pm2, \ldots$ correspond to the sideband instabilities. It should be noted that the influence trends of speed fluctuation on original and sideband instabilities may be different. Based on the first-order perturbation solution, the instability width with different speed fluctuation parameters can be easily obtained. For the second speed fluctuation type, variations of original and sideband instability width of $2\omega_5$ with speed fluctuation parameters are shown in Figure 14, for example. Based on these figures, speed fluctuation parameters can be easily determined to minimize certain instability. Comparing point B ($P = 24.05$ and $\alpha = 0.1$) with point C ($P = 24$ and $\alpha = 0.05$), although speed fluctuation amplitude of point B is larger than point C, the corresponding instability region of point B is much smaller. The numerical results in Figure 15 show the similar decrease when the speed fluctuation is changed from point C to point B.

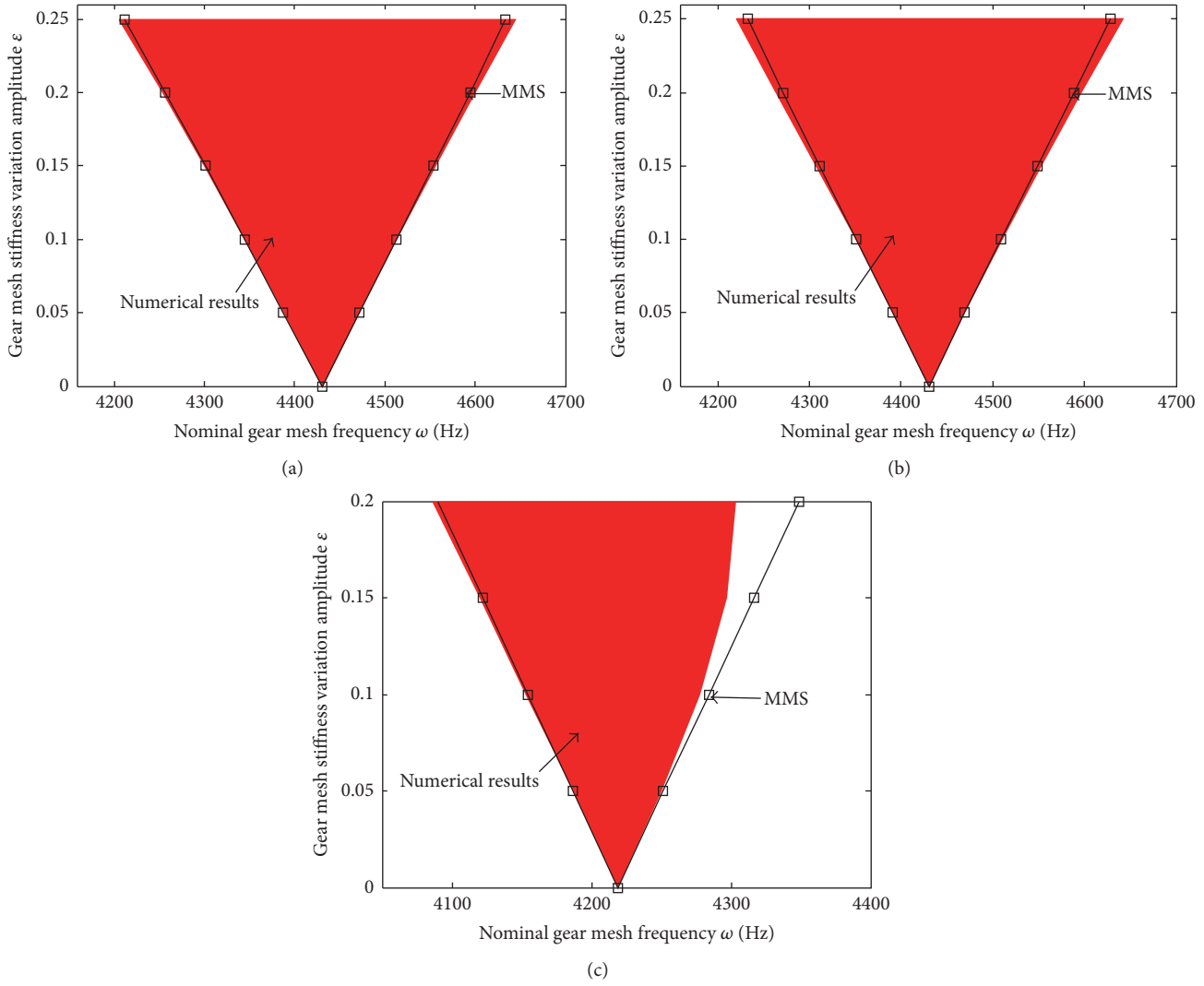

Figure 10: Comparisons of numerical and analytical results: (a) $\alpha = 0.05$ and $\omega_a = 200$ Hz; (b) $\alpha = 0.05$ and $P = 24$; (c) $\alpha = 0.1$ and $P = 20$.

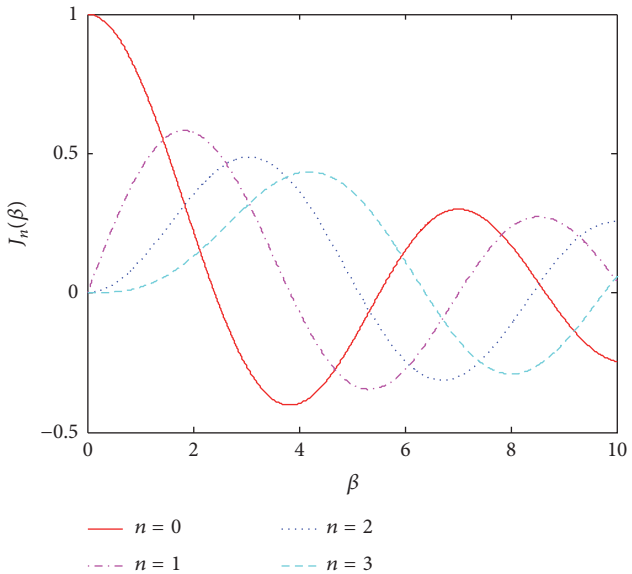

Figure 11: Plot of Bessel function of the first kind for integer orders $n = 0, 1, 2, 3$.

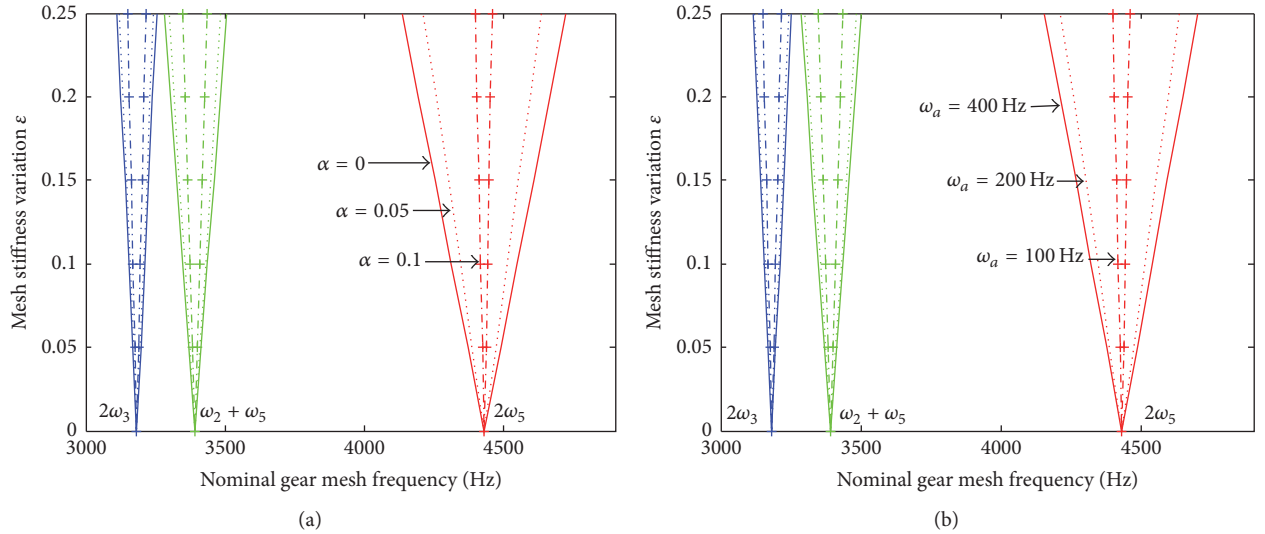

FIGURE 12: Influence of fluctuation amplitude and fluctuation frequency on the original instabilities for the first speed fluctuation type: (a) ω_a = 200 Hz; (b) α = 0.05.

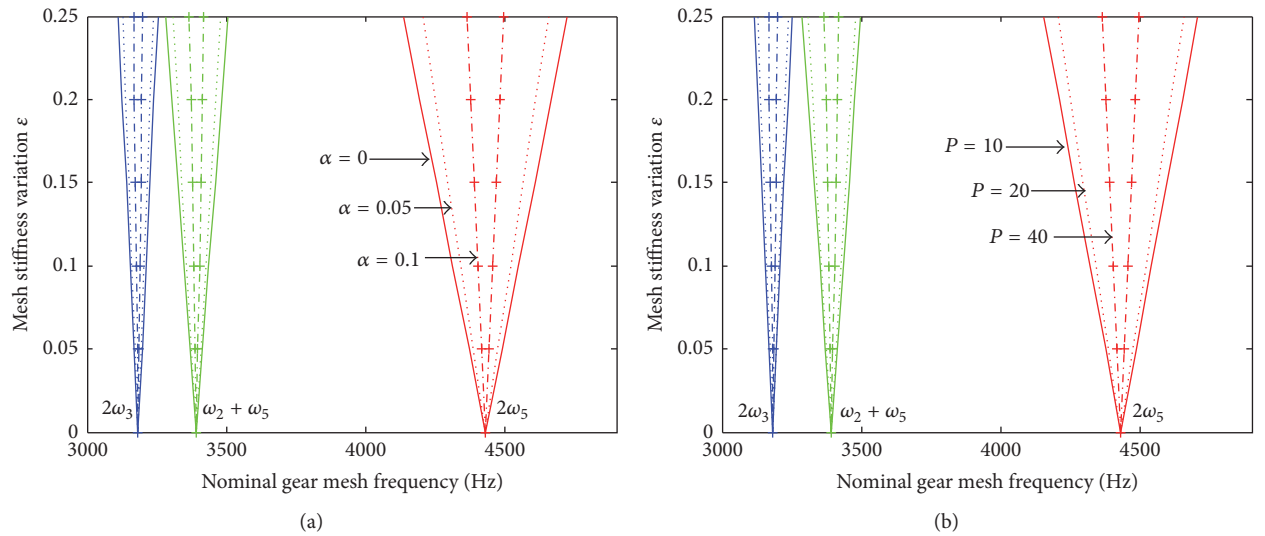

FIGURE 13: Influence of fluctuation amplitude and fluctuation frequency on the original instabilities for the second speed fluctuation type: (a) P = 20; (b) α = 0.05.

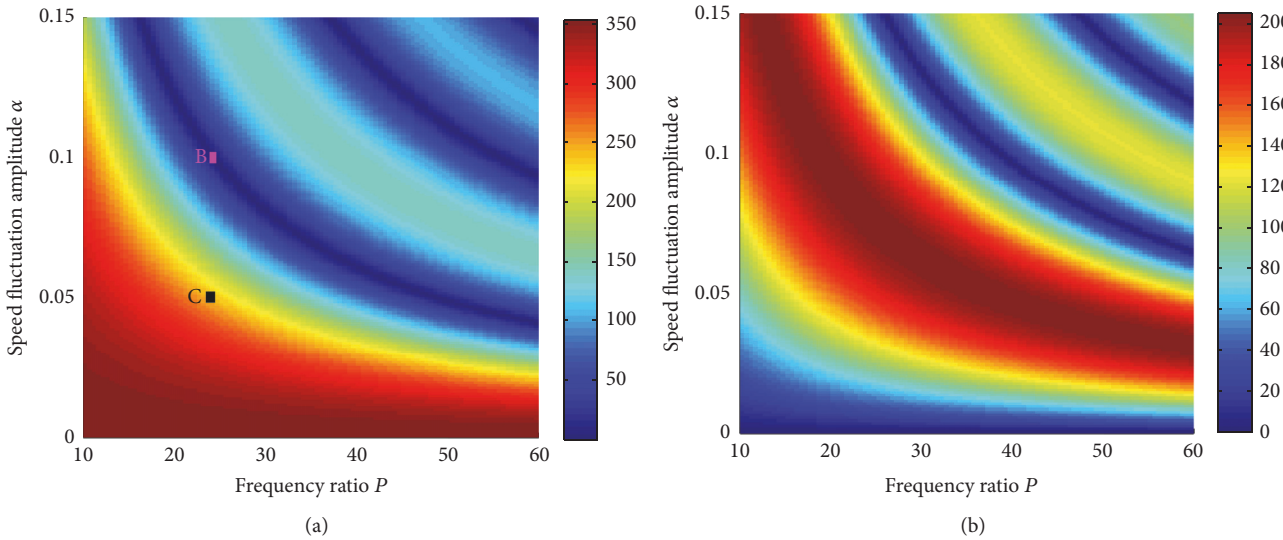

FIGURE 14: Analytical results of (a) original and (b) sideband instability width of $2\omega_5$ with different speed fluctuation parameters for ε = 0.15.

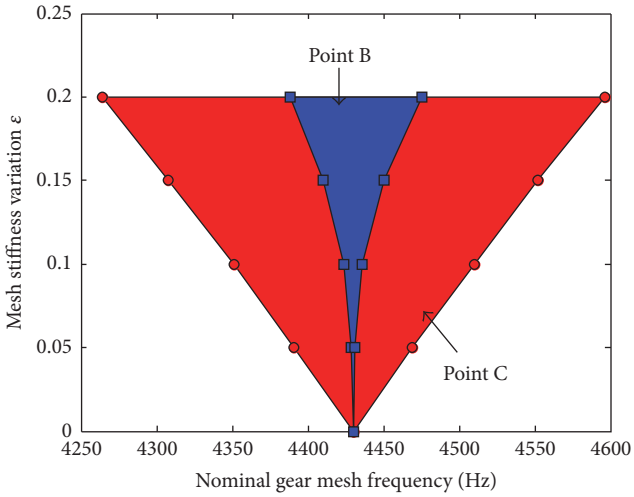

FIGURE 15: Original instability of $2\omega_5$ under different speed fluctuation parameters obtained by numerical integration.

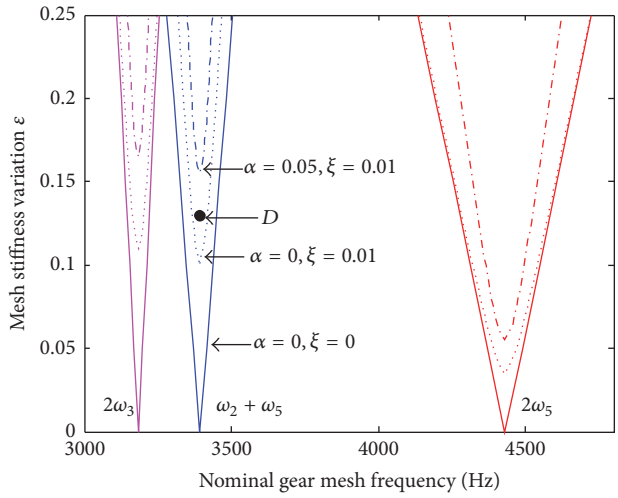

FIGURE 16: Combined effect of the damping and speed fluctuation on original instabilities for $P = 24$ and $\boldsymbol{\xi} = [0,\ 0.01,\ 0.01,\ 0.01,\ 0.01]$.

5.2. Combined Effect of Damping and Speed Fluctuations. In all of the above calculations, damping is constrained to be zero. Taking damping into account, the combined effect of damping and speed fluctuations on original instabilities is shown in Figure 16. It is well known that damping shrinks the instability region for the constant speed. With the inclusion of speed fluctuations, original instability regions are further shrunken. This is because $J_0(\beta)$ obtains its maximum value when the speed is constant ($\beta = 0$). The minimum value $\varepsilon_{\min}$ of the mesh stiffness variance corresponding to the occurrence of original instability is affected by damping and speed fluctuation. As shown in Figure 16, the minimum value for fluctuating speed is larger than that for constant speed. This phenomenon can be easily explained by analytical solutions (see (22), (26), and (29)), and speed fluctuation offers a new way to suppress the occurrence of parametric instability under determined mesh stiffness variation besides increasing the system damping. Taking point D ($\omega = 3393$ Hz and $\varepsilon = 0.13$) in Figure 16 as an example, parametric instability occurs at point D for constant speed ($\alpha = 0$), while the instability is suppressed when speed fluctuation is added ($\alpha = 0.05$). Comparing the minimum stiffness variation $\varepsilon_{\min}$ in three instability regions, it can be found that speed fluctuation has greater influence on the larger instability region.

The influence of speed fluctuation amplitude α on the original and sideband instabilities in the presence of damping is shown in Figure 17. It can be clearly seen that the original instability shrinks, while the sideband instabilities expand with the increase of α for the two speed fluctuations. Because $J_{-n}(\beta) = (-1)^n J_n(\beta)$ and $\omega = P\omega_a$, the minimum values of ε for the corresponding sideband instabilities for the second fluctuation type are equal, while for the first fluctuation type, the ratio of the nominal gear mesh frequency ω and fluctuation frequency ω_a changes with ω, and therefore the minimum values of ε for the corresponding sideband instabilities are not the same.

6. Conclusions

In this study, parametric instabilities of the planetary gear under two different speed fluctuations are systematically investigated. A rotational model of the planetary gear and the mesh stiffness modeling are introduced first. Perturbation analysis is then conducted to determine operating conditions leading to instabilities and the results are verified by numerical integration. Finally, the influences of speed fluctuation parameters and damping on instabilities are investigated, and a new way to control instabilities by adjusting speed fluctuation is proposed. Main conclusions are summarized as follows:

(1) Speed fluctuations induce frequency modulation of the gear mesh stiffness and then cause sideband instabilities on both sides of original instabilities and greatly influence the widths of original instabilities.

(2) Because of the influence of sideband frequencies, whether parametric instability occurs at certain nominal gear mesh frequency cannot be simply predicted by the planet meshing phases that are applicable to constant speed.

(3) The influence of speed fluctuations on instabilities is determined by the Bessel function of the first kind with different order. Original and sideband instabilities can be controlled by changing the value of the corresponding Bessel function, which is realized by adjusting the amplitude and frequency of speed fluctuations.

(4) Damping and speed fluctuations have a combined effect on the occurrence of original instabilities. When the mesh stiffness variation is determined, original instabilities can be suppressed by introducing proper speed fluctuation besides increasing damping.

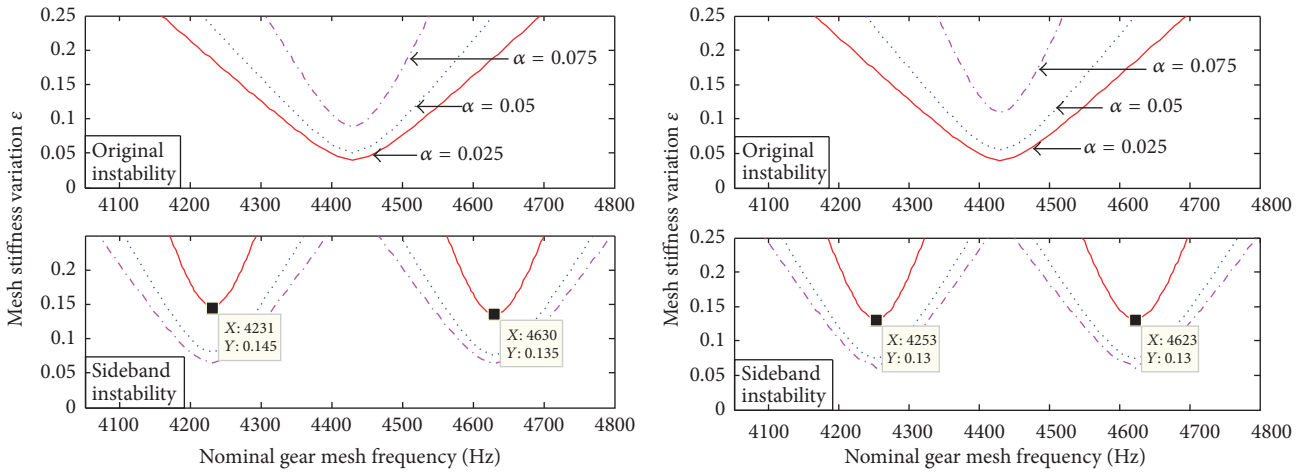

FIGURE 17: Original and sideband instabilities of $2\omega_5$ with $\xi_5 = 0.01$ for different fluctuation type: (a) $\omega_a = 200$ Hz; (b) $P = 24$.

Nomenclature

c_r, c_s: Contact ratios
I_h $(h = c, r, s, 1, \ldots, N)$: Moments of inertia
k_{sn} $(n = 1, \ldots, N)$: Time-varying sun-planet mesh stiffness
k_{sp}: Average sun-planet mesh stiffness
k_{sv}: Variation amplitude of sun-planet mesh stiffness
k_{rn} $(n = 1, \ldots, N)$: Time-varying ring-planet mesh stiffness
k_{rp}: Average ring-planet mesh stiffness
k_{rv}: Variation amplitude of ring-planet mesh stiffness
N: Number of planets
P: Ratio of nominal gear mesh frequency and speed fluctuation frequency
r_h $(h = c, r, s, 1, \ldots, N)$: Base radii
u_h $(h = c, r, s, 1, \ldots, N)$: Rotational displacements
Z_r, Z_s: Tooth number of the ring and the sun
ψ_n: Circumferential angle of the nth planet
φ_h $(h = c, r, s, 1, \ldots, N)$: Rotations in radian
Ω_0: Nominal input speed
α: Variation amplitude of input speed fluctuation
α_s, α_r: Pressure angles
γ_{sn}, γ_{rn}: Planet meshing phase
ω_a: Frequency of speed fluctuation
ω: Nominal gear mesh frequency
$\varepsilon_1, \varepsilon_2$: Relative amplitude of gear mesh stiffness variation
ξ: Modal damping ratio
σ: Detuning parameter.

Subscript

c: Carrier
n: nth planet
r: Ring
s: Sun.

Conflicts of Interest

The authors declare that they have no conflicts of interest.

Acknowledgments

The research work described in this paper was supported by the National Natural Science Foundation of China under Grant no. 51335006 and Beijing Natural Science Foundation under Grant no. 3131002.

References

[1] P. Velex and L. Flamand, "Dynamic response of planetary trains to mesh parametric excitations," *Journal of Mechanical Design*, vol. 118, no. 1, pp. 7–14, 1996.

[2] M. Botman, "Vibration measurements on planetary gears of aircraft turbine engines," *Journal of Aircraft*, vol. 17, no. 5, pp. 351–357, 1980.

[3] V. K. Ambarisha and R. G. Parker, "Nonlinear dynamics of planetary gears using analytical and finite element models," *Journal of Sound and Vibration*, vol. 302, no. 3, pp. 577–595, 2007.

[4] J. Lin and R. G. Parker, "Analytical characterization of the unique properties of planetary gear free vibration," *Journal of Vibration and Acoustics*, vol. 121, no. 3, pp. 316–321, 1999.

[5] J. Lin and R. G. Parker, "Structured vibration characteristics of planetary gears with unequally spaced planets," *Journal of Sound and Vibration*, vol. 233, no. 5, pp. 921–928, 2000.

[6] J. Lin and R. G. Parker, "Planetary gear parametric instability caused by mesh stiffness variation," *Journal of Sound and Vibration*, vol. 249, no. 1, pp. 129–145, 2002.

[7] G. V. Tordion and R. Gauvin, "Dynamic stability of a two-stage gear train under the influence of variable meshing stiffnesses," *J Eng Ind Trans ASME*, vol. 99, no. 3, pp. 785–791, 1977.

[8] M. Benton and A. Seireg, "Normal mode uncoupling of systems with time varying stiffness," *Journal of Mechanical Design, Transactions of the ASME*, vol. 102, no. 2, pp. 379–383, 1980.

[9] J. Lin and R. G. Parker, "Mesh stiffness variation instabilities in two-stage gear systems," *Journal of Vibration and Acoustics*, vol. 124, no. 1, pp. 68–76, 2002.

[10] D. L. Seager, "Conditions for the neutralization of excitation by the teeth in Epicyclic Gearing," *Journal of Mechanical Engineering Science*, vol. 17, no. 5, pp. 293–298, 1975.

[11] A. Kahraman and G. W. Blankenship, "Planet mesh phasing in epicyclic gear sets," in *Proceedings of the International Gearing Conference*, pp. 99–104, Newcastle, U.K, 1994.

[12] A. Kahraman, "Planetary gear train dynamics," *Journal of Mechanical Design, Transactions of the ASME*, vol. 116, no. 3, pp. 713–720, 1994.

[13] R. G. Parker, "Physical explanation for the effectiveness of planet phasing to suppress planetary gear vibration," *Journal of Sound and Vibration*, vol. 236, no. 4, pp. 561–573, 2000.

[14] R. G. Parker and X. Wu, "Parametric instability of planetary gears having elastic continuum ring gears," *Journal of Vibration and Acoustics*, vol. 134, no. 4, Article ID 041011, 2012.

[15] G. Sika and P. Velex, "Analytical and numerical dynamic analysis of gears in the presence of engine acyclism," *Journal of Mechanical Design, Transactions of the ASME*, vol. 130, no. 12, pp. 1245021–1245026, 2008.

[16] G. Sika and P. Velex, "Instability analysis in oscillators with velocity-modulated time-varying stiffness—applications to gears submitted to engine speed fluctuations," *Journal of Sound and Vibration*, vol. 318, no. 1-2, pp. 166–175, 2008.

[17] X. Qiu, Q. Han, and F. Chu, "Analytical investigation on unstable vibrations of single-mesh gear systems with velocity-modulated time-varying stiffness," *Journal of Sound and Vibration*, vol. 333, no. 20, pp. 5130–5140, 2014.

[18] X. Qiu, Q. Han, and F. Chu, "Parametric instability in planetary gears with frequency-modulated time-varying mesh stiffness," in *Proceedings of the ASME 2014 International Design Engineering Technical Conferences and Computers and Information in Engineering Conference, IDETC/CIE 2014*, New York, NY, USA, 2014.

[19] C. Bahk and R. G. Parker, "Analytical solution for the nonlinear dynamics of planetary gears," *Journal of Computational and Nonlinear Dynamics*, vol. 6, no. 2, Article ID 021007, pp. 1–15, 2011.

[20] A. H. Nayfeh and D. T. Mook, *Nonlinear Oscillations*, John Wiley & Sons, New York, NY, USA, 1979.

[21] C. N. Moore, "The summability of the developments in Bessel functions, with applications," *Transactions of the American Mathematical Society*, vol. 10, no. 4, pp. 391–435, 1909.